Large eddy simulation of a stenosed artery

T. J. Barber[1] A. Simmons[2]

(Received 31 January 2010; revised 21 April 2010)

Abstract

A large eddy simulation is conducted of a 50% stenosed artery. The inlet boundary condition is a physiologically accurate pulsatile flow, representative of that found in a femoral artery. The transient, three dimensional results show the non-axisymmetric nature of the flow field; high values of wall shear stress, oscillatory in both space and time are also observed. The identification of such fluid dynamic quantities within a stenosed vessel is important in understanding the likely causes and ongoing effects on the integrity of the vessel.

Contents

http://anziamj.austms.org.au/ojs/index.php/ANZIAMJ/article/view/2550 gives this article, © Austral. Mathematical Soc. 2010. Published May 7, 2010. ISSN 1446-8735. (Print two pages per sheet of paper.)

1 Introduction

Arterial stenosis refers to a condition in which a narrowing of the artery exists which causes a disruption in the blood flow, and in severe stenosis, turbulent flow. The analysis of fluid dynamic quantities such as velocity profiles, turbulent quantities and wall shear stress (WSS) are important in gaining an understanding of the mechanisms that may contribute to conditions such as atherosclerosis, which causes arterial stenosis, and also the effects on the vessel from the changed flow conditions downstream of a stenosis. In vivo measurement of these data is difficult; computational simulation is proving to be a useful methodology for gaining such information. While regions of both high and low shear stress have been highlighted as potential atherosclerotic development sites, how rapidly the WSS varies in space and time is of most significance. Fluid shear stresses in healthy large arteries are typically 1–2 Pa [1]; however, shear stresses may be as large as 200 Pa in the narrowed throat region of a severely stenosed artery [2].

In stenosed vessel flows, turbulence is likely to occur downstream of the stenosis, even for moderate Reynolds numbers [1]. Turbulent flow in a blood vessel has considerable implications for the integrity of the vessel, particularly the effect on the wall shear stress.

Pulsatile stenotic flows have been the focus of a number of numerical simulations in the past decade, ranging from standard Reynolds Averaged Navier Stokes (RANS) solutions [3] to computationally intensive Direct Numerical Simulation (DNS) models [4]. Not unexpectedly, given the large computational resources required, the DNS models are generally channels, representing a simplified stenosed artery flow. RANS CFD solutions utilised a range of two equation models for the turbulence closure, with the k-ω model comparing well [3, 5] to the frequently cited experimental results of Giddens and

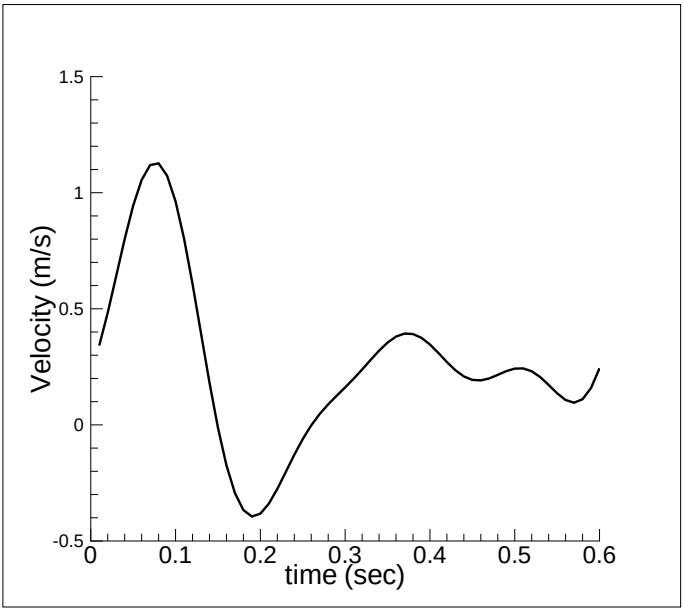

FIGURE 1: Femoral profile

colleagues [6]. These in vitro experiments, using Laser Doppler Anemometry and flow visualization produced useful data relating to the post-stenotic flow behaviour for vessels with a range of stenoses. Large Eddy Simulation (LES) models [11], providing a middle ground in complexity and computational resources, are proving to be useful in determining fine details of flow structures for pulsatile arterial stenosis flows. For a stenosed channel flow [7] the LES sub-grid model can dissipate around 23% of the energy of the flow, mostly in the post-stenotic region, justifying the use of this more complex model for this type of problem.

A computational analysis is conducted of a rigid, symmetric artery with a 50% stenosis, for a physiological pulsatile profile, representative of the femoral artery [8]. The profile, shown in Figure 1, represents one cycle and is

given in terms of axial velocity distribution over time, as this is the form in which the profile is specified in the computational model. At the beginning of the cycle ($t = 0\,s$), the fluid travels forward at approximately $0.2\,m\,s^{-1}$ and quickly increases axial velocity to the peak systole value of $1.16\,m\,s^{-1}$ at $t = 0.08\,s$. After this peak value is reached, the axial velocity drops sharply and enters the diastole stage of the cycle, with a peak (reverse direction of flow) axial velocity of $0.4\,m\,s^{-1}$. From this point, a gradual increase (with two smaller drops in magnitude) is found until the end of the cycle at $0.6\,s$.

Results are given in the form of contours of axial velocity, vorticity magnitude and WSS. The three dimensionality of the flow field is apparent, as is the strong downstream core formed at peak systole. Recirculation zones and the subsequent breakup of the shear layers indicate regions of high WSS.

2 Methodology

The modelled geometry, representing a simplified stenosed artery, consists of a $D = 10\,mm$ diameter axisymmetric cylindrical domain, with a 50% occluded axisymmetric stenosis, with an extent of $2D$ from start to end. The modelled region extends $5D$ before the stenosis begins, and extends $15D$ beyond the stenosis. The effect of the extent of the domain was not studied during the validation and verification process due to computational resource limitations; however, the results show that the domain should be larger. The flow is assumed to be incompressible, homogenous and Newtonian with the fluid properties approximating blood (density of $1.06 \times 10^3\,kgm^{-3}$ and viscosity of $3.71 \times 10^{-3}\,m^2s^{-1}$). Newtonian flow in vessels of this size has been shown to be a reasonable assumption [9]. The vessel walls are assumed rigid. Distances quoted as 'downstream' or 'upstream' of the stenosis are taken from the end of the stenosis (not the centre).

The pulsatile profile is representative of the profile found in a femoral artery. Figure 1 gives the inlet velocity profile as modelled and is of particular in-

terest given the significant flow reversal during the diastolic phase. The inlet conditions were set as plug flow (uniform across the inlet); a parabolic, fully developed profile is not appropriate for velocity conditions that may experience flow reversal. All vessel walls are set to non-slip boundaries and the downstream outlet is an open boundary that allows both forward and reverse flow.

A fully structured mesh was produced, with mild bias towards the walls to enable capture of boundary layer development and also mild bias from both the inlet and outlet towards the region of the stenosis. The mesh consisted of 15 blocks of structured hexahedral cells, giving a total number of cells of 5.7 million. A timestep of 0.001 s was used, resulting in a Courant number of approximately 0.2, and the residual error level within each timestep, for each equation, was 10^{-5}. The Reynolds number was calculated based on stenosis diameter and peak inlet velocity, giving $\mathrm{Re} = 1600$. The computational models were run in parallel across 32 nodes on an SGI Altix 4700 64 bit shared memory machine, with 128 Dual-Core 1.6 GHz CPUs and 1 Tbyte RAM. All cases were run with double precision accuracy.

The filtered Navier–Stokes equations were solved using a commercial finite volume code, Fluent 6.3. The sub-grid scale stresses are modelled using the dynamic Smagorinsky–Lilly model via the Boussinesq hypothesis [10]. In this model, Smagorinsky's eddy viscosity formulation is used; however, the square of the Smagorinsky constant is replaced by a coefficient. For a case of boundary layer flow, Geurts [11] finds that the dynamic model produces excellent accuracy with a significant saving of computational effort, when compared to DNS results.

The initial condition was set from a steady state RANS k-ϵ solution, for a velocity equal to the pulsatile velocity at $t = 0$. Momentum equations were solved by central differencing and pressure-velocity coupling achieved with the PISO scheme. Six full pulsatile cycles were completed before any data was collected; however, the effect of further cycles was not investigated and it is possible the flow may not have fully settled by this stage.

3 Results and discussion

Axial velocity contours along a midplane are given in Figure 2. The peak velocity occurring in the region is $4.5\,\mathrm{m\,s^{-1}}$ and is found at the time of peak systole. Contour plots are given at six points in the cycle (each $0.1\,\mathrm{s}$) in order to capture the transient nature of the flow. At $t = 0.1\,\mathrm{s}$, the cycle is near peak systole and a reasonably uniform flow observed, with a central core of high speed fluid moving downstream of the stenosis, surrounded by sections of slow reverse (negative x direction) flow. The core is well contained and the shear layers do not thicken considerably in the region shown. At $t = 0.2\,\mathrm{s}$, the cycle has reached peak diastole, and most of the fluid is moving in the reverse direction. Again, a core of fast moving fluid is observed (now on the left side of the stenosis).

Regions of forward moving fluid are seen on either side of the core and downstream of the stenosis, where non-axisymmetric flow is also apparent. At $t = 0.3\,\mathrm{s}$, the fluid is again moving in the forward direction but at a relatively slow velocity and this is reflected in the contour plot where a slightly faster region of flow is seen at the stenosis. A small amount of reversed flow remains upstream of the stenosis, where the fast moving core existed at the earlier time step. Moving forward to $t = 0.4\,\mathrm{s}$, the fluid has recovered from the diastole part of the cycle and the only reversed sections of flow are seen after the stenosis, on either side of the core flow. For the last section of the cycle ($t = 0.5\,\mathrm{s}$ and $t = 0.6\,\mathrm{s}$) the velocity stays fairly constant with a faster central core of around $1\,\mathrm{m\,s^{-1}}$ which shows some degree of three dimensionality, surrounded by slower (reversed for at $t = 0.5\,\mathrm{s}$) regions and very uniform upstream flow.

A representation of the full flow field is given in Figure 3, in which the distribution of axial velocity over time (x-axis) and distance (y-axis) is given. The image is constructed from data collected at every timestep, on a line along the centre line of the vessel. The centre of the stenosis is located at $y = 0.06\,\mathrm{m}$ and the effect of this geometry clearly seen in the figure. The red

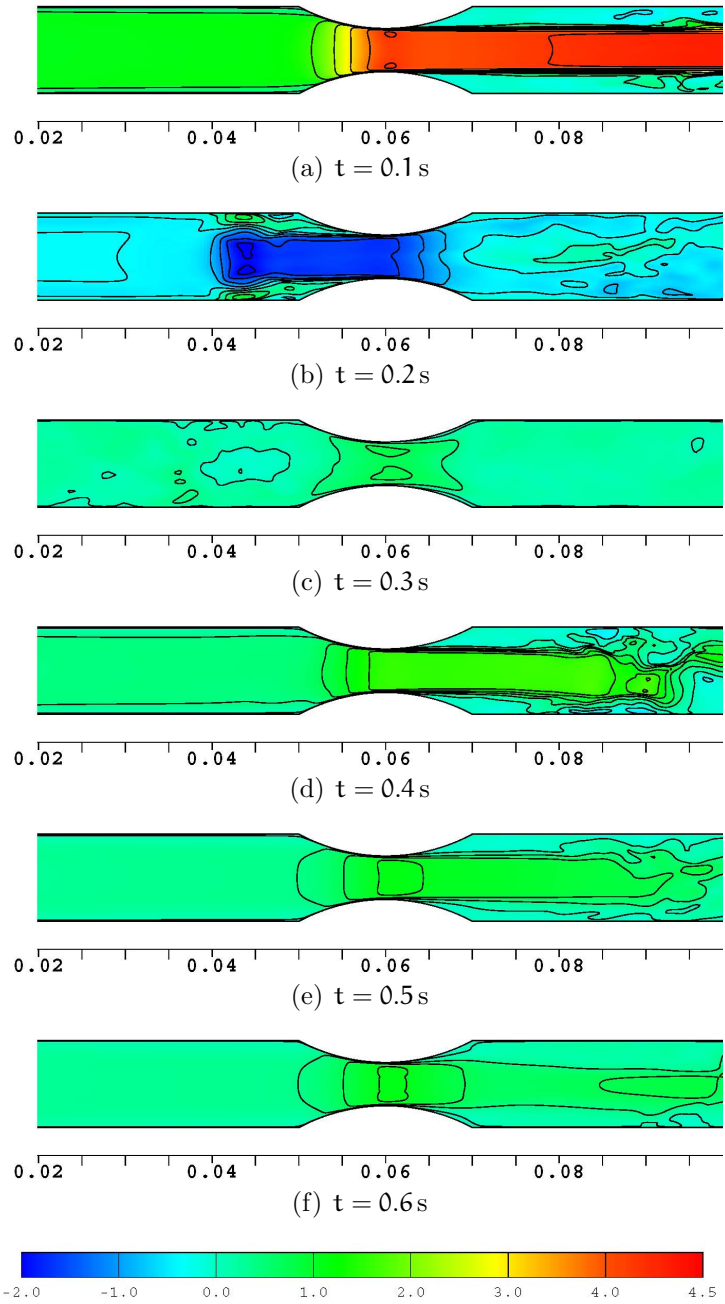

FIGURE 2: Axial Velocity ($\mathrm{m\,s^{-1}}$) on mid-plane over the cycle.

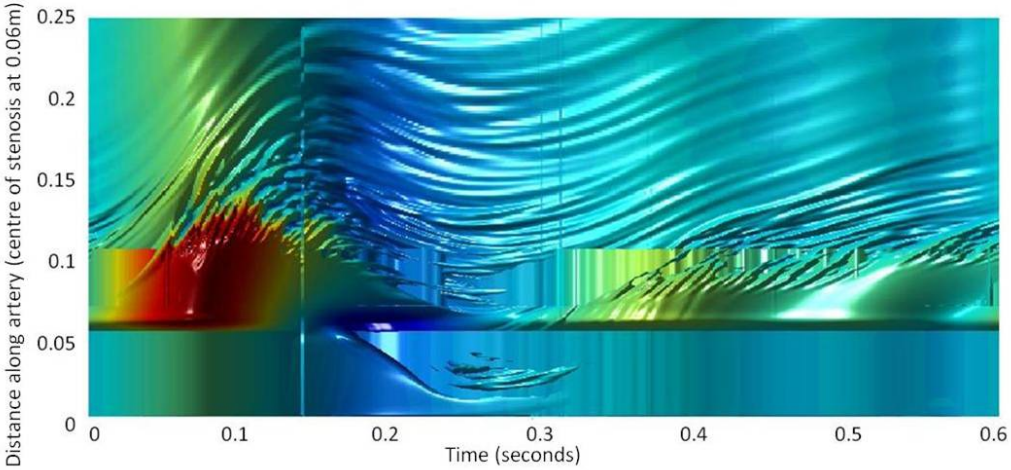

FIGURE 3: Spatio-temporal distribution of axial velocity (scale as previous)

region in the lower left of the image represents the high speed peak systole section of the cycle and the disturbance to the flow is seen to be far reaching, both spatially and temporally. As the data collected is from cycle seven, the effects of the previous flow cycle are seen at the left side of the image. However, at the upper region of the figure the flow disturbance propagates to the downstream boundary, indicating that this boundary may not be located at a far enough distance downstream and further work is being conducted to assess this. Upstream disturbances close to the boundary appear minimal.

Figure 4 shows more detail of these features. It shows contours of vorticity magnitude on the same plane at the same points in the cycle. The defined shear layer separating the central core of fluid is clearly seen for $t = 0.1\,s$, with the shear layer staying well defined until around 2D downstream of the stenosis when some breakup in the outer region can be noted. Vorticity levels increase in the outer region of the vessel as the shear layer breaks up.

At $t = 0.2\,s$ (peak diastole) high values of vorticity occur upstream of the

stenosis, and there is evidence of disturbed flow downstream. The asymmetric and well defined nature of the upstream vortex ring is clearly seen in this image. In the next image, little vorticity is found in the fluid as the velocity has slowed, the upstream vortex ring has dissipated and the downstream flow is still to be established. By $t = 0.4\,s$ this downstream flow is well established and as in the initial image a clear shear layer occurs. However, due to the slower velocity at this time in the cycle compared to that found at $t = 0.1\,s$, the breakup occurs much earlier and the region outside the inner core experiences a greater level of vorticity and disturbed flow not far beyond the stenosis. In the later two images ($t = 0.5\,s$ and $t = 0.6\,s$) the shear layer continues to die down and vorticity gradually dissipates as the fluid velocity slows.

Figure 5 shows a representation of the full flow field for vorticity and for subgrid scale (SGS) turbulent viscosity (an indication of the turbulence in the flow field as it links the subgrid scale stresses to the gradients of filtered velocity). The distributions over time (x axis) and distance (y axis) are given, as for Figure 3.

As expected, regions of high vorticity are seen near the time of peak systole, and some less high values found for the peak diastole region. The breakdown of the systole core shear layer is apparent in the high values of vorticity seen downstream (higher on the y axis) of the stenosis. In comparison to the axial velocity field, the vorticity is more contained within the high value regions and does not extend as far either temporally or spatially. In contrast, the SGS viscosity distribution shows disturbances to propagate well within the domain, easily reaching the downstream extent of the model. This image shows that the modelled domain is required to be significantly longer. The effect of biasing the size of the cells is also apparent; the image appears somewhat pixelated near the downstream boundary and this is very likely to be a result of the larger cell size in this region.

Finally, wall shear stress (WSS) is considered, by plotting a contour of WSS along a plane of angular distance around the diameter (in the y-direction)

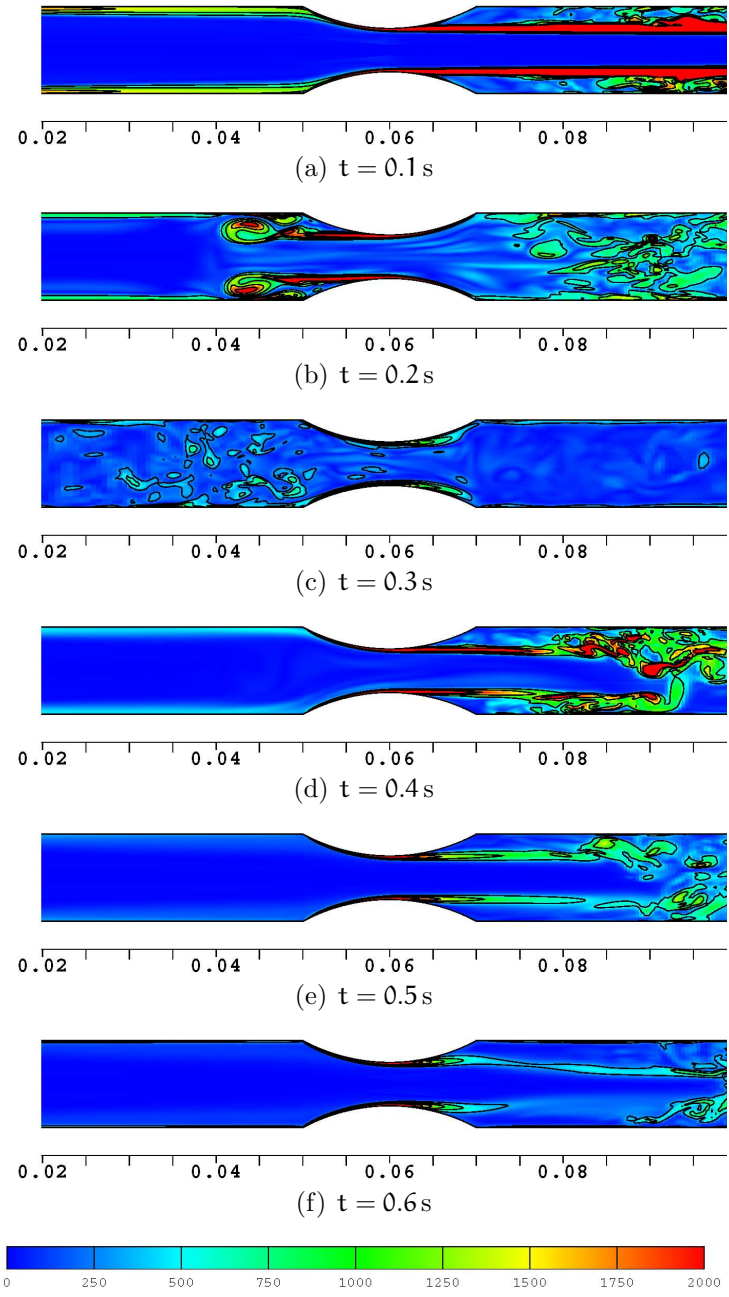

FIGURE 4: Vorticity Magnitude(s^{-1}) on mid-plane over the cycle.

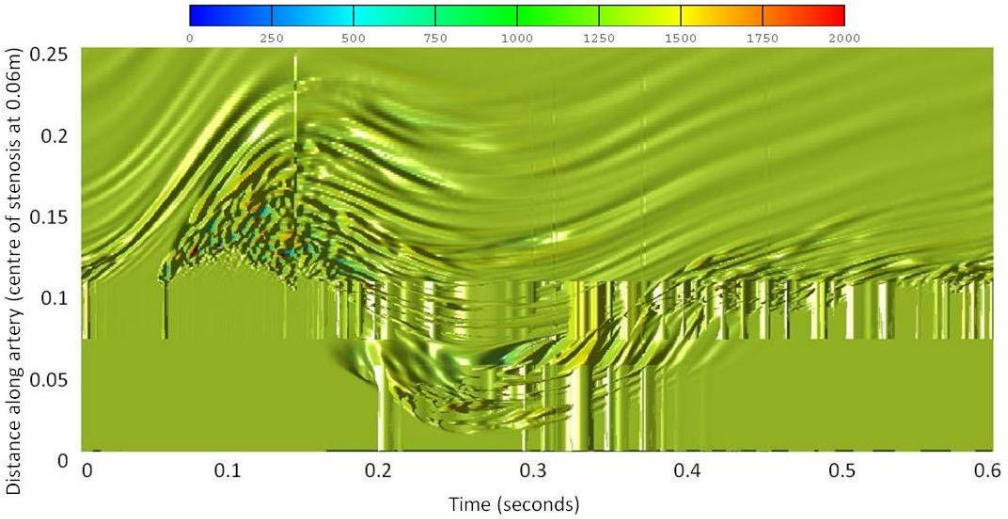

(a) vorticity

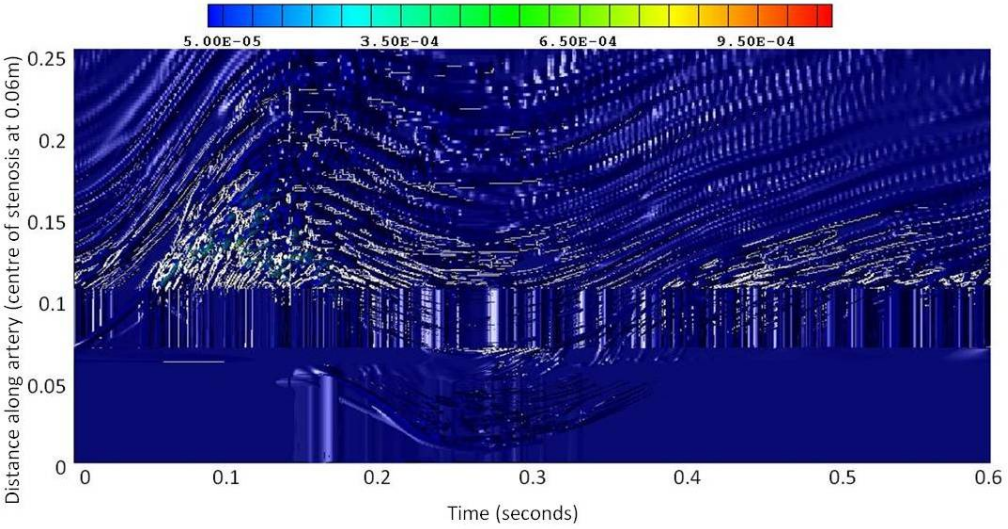

(b) subgrid scale viscosity

FIGURE 5: Spatio-temporal distribution of vorticity and subgrid scale viscosity

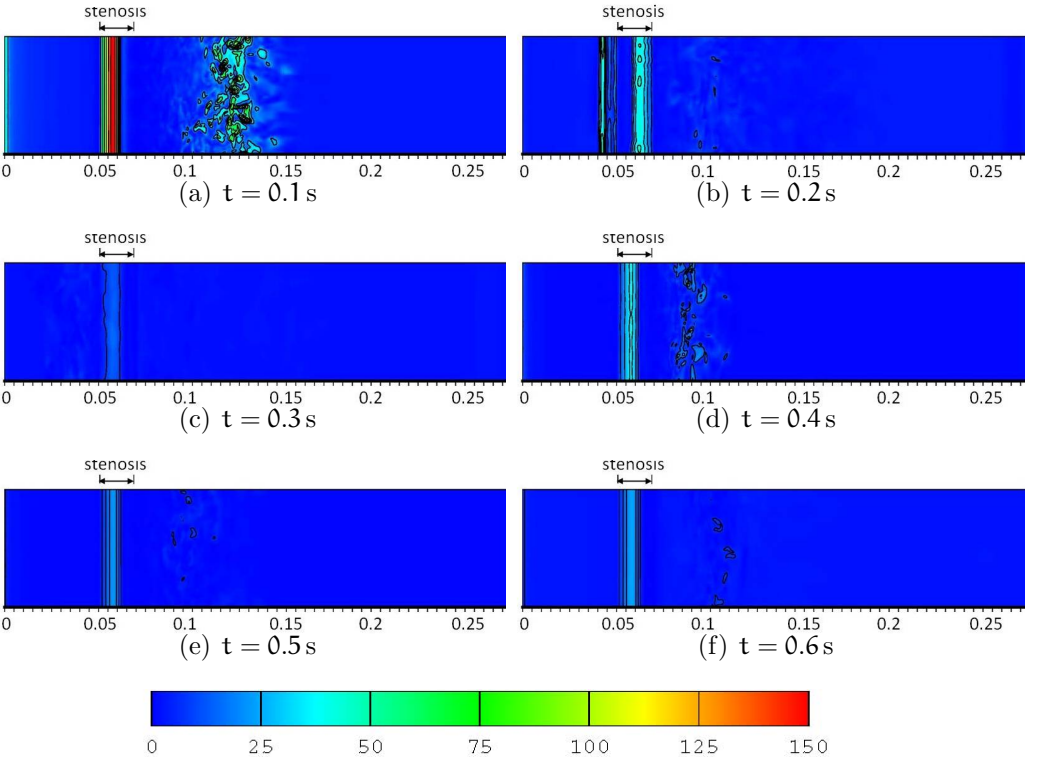

FIGURE 6: Wall Shear Stress (Pa) over the cycle.

and vessel length (in the x-direction). This allows the vessel wall to be 'opened out' (Figure 6). The location of the stenosis is shown on each image. Highest levels of WSS are found when the fluid is at the peak systole stage of the cycle, driving the greatest amount of fluid through the small region of the stenosis. Consequently, values of WSS of 150 Pa are found on the walls within the stenosis. Also in the downstream region (approximately 5D from the stenosis), where the shear layer has started to break apart and create disturbed flow outside of the central core, high levels of WSS are found, up to 150 Pa in small sections. The extent of this disturbed downstream region extends for around 4D, with very low or zero levels of WSS either side. Upstream of the stenosis, the WSS also quickly returns to a small value. For all six timepoints examined within the cycle, elevated values of WSS are found in the stenosis region, though these values drop to 15 Pa at $t = 0.3$ s. During the diastole section of the cycle, seen for the timestep of $t = 0.2$ s, WSS values of 50 Pa are seen at a location approximately 1D upstream from the stenosis. At the remaining points within the cycle, the WSS remains at a low value for the region before and after the stenosis.

4 Conclusions

A three dimensional Large Eddy Simulation was conducted of a 50% occluded vessel, with a typical femoral artery profile used as the transient inlet conditions; the fluid was assumed to be homogenous, Newtonian and incompressible and the walls are assumed rigid. During systole, a central core of high speed fluid was observed moving downstream of the stenosis, surrounded by sections of slow reverse flow; during diastole, again, a core of fast moving fluid is observed, now on the upstream side of the stenosis. Regions of high vorticity are seen near the time of peak systole, and some less high values found for the peak diastole region. For the relatively mild case of a 50% occluded vessel, the computed results for WSS indicate that over one cycle the WSS will oscillate from 15 Pa to 150 Pa in the region of the stenosis.

Downstream of the stenosis, where the breakup of the fast moving central core is found, WSS values also fluctuate from less than 5 Pa to 150 Pa. In this region, the high values of WSS are not uniform across the diameter (due to the non-asymmetric breakup of the core) and therefore oscillations within the one cycle would also be expected. LES has been shown to be a feasible option for the study of stenosed arterial flows, allowing detailed temporal, three dimensional characteristics to be captured. Due to the computationally intense nature of the simulations, the extent of the geometry was restricted in length; the results indicate that both upstream and downstream boundaries should be located further away from the stenosis. In particular, the spatio-temporal graph of subgrid scale viscosity clearly showed the turbulent flow disruption extended beyond the length of the domain in the downstream direction. Further work is being conducted to further refine the results.

References

[1] S. A. Berger and L-D. Jou. Flows in Stenotic Vessels. *Annu. Rev. Fluid Mech.* 32:347–382. 2000. doi:10.1146/annurev.fluid.32.1.347 C187

[2] M. Li, J. Beech-Brandt, L. John, P. Hoskins, W. Easson. Numerical Analysis of Pulsatile Blood Flow and Vessel Wall Mechanics in Different Degrees of Stenoses. *J. Biomechanics* 40:3715–3724. 2007. doi:10.1016/j.jbiomech.2007.06.023 C187

[3] S. S. Varghese and S. H. Frankel. Numerical Modeling of Pulsatile Turbulent Flow in Stenotic Vessels. *J. Biomech. Eng.* 125 (445–460). 2003. doi:10.1115/1.1589774 C187

[4] S. S. Varghese, S. H. Frankel and P. F. Fischer. Direct numerical simulation of stenotic flows. Part 2. Pulsatile flow. *Journal of Fluid Mechanics.*, 582:281–318. 2007. doi:10.1017/S0022112007005836 C187

[5] B. Xiao and Y. Zhang. Numerical simulation of pulsatile turbulent flow in tapering stenosed arteries. *Int. J. Numerical Meth. Heat Fluid Flow*, 19(5):561–573. 2009. doi:10.1108/09615530910963526 C187

[6] B. Lieber and D. Giddens. Post-stenotic core flow behavior in pulsatile flow and its effects on wall shear stress. *J. Biomech.*, 23(6):597–605. 1990. doi:10.1016/0021-9290(90)90052-5 C188

[7] M. Paul, Md. M. Molla and G. Roditi. Large eddy simulation of pulsatile blood flow. *Medical Engineering and Physics*, 31:153–159. 2009. doi:10.1016/j.medengphy.2008.04.014 C188

[8] W. W. Nichol and M. F. O'Rourke. *McDonald's Blood Flow in Arteries: Theoretical, Experimental and Clinical Principles*, Hodder Arnold, London, 5th edition. 2005. C188

[9] D. N. Ku. Blood flow in arteries. *Annu. Rev. Fluid Mech.* 29:399–434. 1997. doi:10.1146/annurev.fluid.29.1.399 C189

[10] D. Lilly. A Proposed Modification of the Germano Subgrid-Scale Closure Model. *Physics of Fluids*, 4:633–635. 1992. doi:10.1063/1.858280 C190

[11] B. Geurts. *Elements of direct and large eddy simulation.* R. T. Edwards, 2004. C188, C190

Author addresses

1. **T. J. Barber**, School Mechanical & Manufacturing Engineering, University of New South Wales, Sydney, Australia.
mailto:t.barber@unsw.edu.au

2. **A. Simmons**, Graduate School of Biomedical Engineering, University of New South Wales, Sydney, Australia.